Clinical Radiology 78 (2023) 687–696

Contents lists available at ScienceDirect

Clinical Radiology

journal homepage: www.clinicalradiologyonline.net

Preoperative prediction of microvascular invasion and perineural invasion in pancreatic ductal adenocarcinoma with ^{18}F-FDG PET/CT radiomics analysis

C. Jiang [a,b,1], Y. Yuan [c,1], B. Gu [a], E. Ahn [d], J. Kim [c], D. Feng [c], Q. Huang [e,*], S. Song [a,**]

[a] *Department of Nuclear Medicine, Fudan University Shanghai Cancer Center, Fudan University, Shanghai, China*
[b] *Department of Nuclear Medicine, The Second Xiangya Hospital, Central South University, Changsha, China*
[c] *Biomedical and Multimedia Information Technology Research Group, School of Computer Science, University of Sydney, Sydney, Australia*
[d] *Discipline of Information Technology, College of Science & Engineering, James Cook University, Australia*
[e] *School of Biomedical Engineering, Shanghai Jiao Tong University, Shanghai, China*

ARTICLE INFORMATION

Article history:
Received 11 October 2022
Received in revised form
23 April 2023
Accepted 13 May 2023

AIM: To develop and validate a predictive model based on 2-[^{18}F]-fluoro-2-deoxy-D-glucose (^{18}F-FDG) positron-emission tomography (PET)/computed tomography (CT) radiomics features and clinicopathological parameters to preoperatively identify microvascular invasion (MVI) and perineural invasion (PNI), which are important predictors of poor prognosis in patients with pancreatic ductal adenocarcinoma (PDAC).

MATERIALS AND METHODS: Preoperative ^{18}F-FDG PET/CT images and clinicopathological parameters of 170 patients in PDAC were collected retrospectively. The whole tumour and its peritumoural variants (tumour dilated with 3, 5, and 10 mm pixels) were applied to add tumour periphery information. A feature-selection algorithm was employed to mine mono-modality and fused feature subsets, then conducted binary classification using gradient boosted decision trees.

RESULTS: For MVI prediction, the model performed best on a fused subset of ^{18}F-FDG PET/CT radiomics features and two clinicopathological parameters, with an area under the receiver operating characteristic curve (AUC) of 83.08%, accuracy of 78.82%, recall of 75.08%, precision of 75.5%, and F1-score of 74.59%. For PNI prediction, the model achieved best prediction results only on the subset of PET/CT radiomics features, with AUC of 94%, accuracy of 89.33%, recall of 90%, precision of 87.81%, and F1 score of 88.35%. In both models, 3 mm dilation on the tumour volume produced the best results.

* Guarantor and correspondent: Q. Huang, School of Biomedical Engineering, Shanghai Jiao Tong University, No. 800 Dongchuan Road, Shanghai 200240, China. Tel.: +8613816622037.
** Guarantor and correspondent: S. Song, Department of Nuclear Medicine, Fudan University Shanghai Cancer Center, Fudan University, No. 270 Dong'an Road, Shanghai 200032, China. Tel.: +8618121299622.
E-mail addresses: qiuhuang@sjtu.edu.cn (Q. Huang), shaoli-song@163.com (S. Song).
[1] These authors contributed equally to this work.

https://doi.org/10.1016/j.crad.2023.05.007

CONCLUSIONS: The radiomics predictors from preoperative ^{18}F-FDG PET/CT imaging exhibited instructive predictive efficacy in the identification of MVI and PNI status preoperatively in PDAC. Peritumoural information was shown to assist in MVI and PNI predictions.

Introduction

Pancreatic cancer is a highly malignant tumour in the digestive system. The 5-year overall survival rate is <6%,[1] and the 5-year survival rate of advanced pancreatic cancer patients is <1%.[2] The most common, pancreatic ductal adenocarcinoma (PDAC), accounts for approximately 90% of pancreatic cancer. Pancreatico-duodenectomy surgery remains the best potential curative treatment; however, the recurrence rate is as high as 25% after 1 year of pancreatico-duodenectomy surgery.[3] It is crucial to find biomarkers that can identify aggressive behaviour of PDAC. Studies have shown that neurovascular invasion (NVI), meaning microvascular invasion (MVI) or perineural invasion (PNI), is the first independent factor affecting the prognosis of pancreatic cancer patients.[4,5] NVI often indicates the invasiveness of the tumour[6,7] and significantly associates with higher risk of early recurrence and metastasis.[8,9] Precise identification of NVI before surgery in patients with PDAC is of critical clinical relevance in arriving at accurate prognostication[10] and guiding more appropriate resection margin to achieve better survival outcomes. Unfortunately, the determinations of MVI and PNI are still based on intraoperative or postoperative pathological diagnosis.

Radiomics that has emerged in recent years brings hope for the preoperative evaluation of MVI and PNI based on medical imaging. Radiomics is a quantitative high-throughput feature extraction method that mines medical images into high-dimensional extractable data[11] and aims to reflect the biological characteristics of tumours. Radiomics data analysis can provide clinical stratification to screen for potential beneficiaries, for example, differentiating patients with potentially resectable tumours from those that are not appropriated for pancreatico-duodenectomy surgery, providing precise diagnosis and treatment.[12] Several radiomics features for the preoperative prediction of MVI and PNI status have been introduced. Peng *et al.*[13] and Zhang *et al.*[14] showed that radiomics nomograms based on contrast-enhanced computed tomography (CECT) images achieved favourable accuracy for preoperative prediction of MVI in patients with hepatocellular carcinoma (HCC). Similarly, Chen *et al.*[15] developed a magnetic resonance imaging (MRI)-based radiomics nomogram for the assessment of PNI status in patients with rectal cancer. The above radiomics features were, however, only extracted from the intra-tumoural regions without considering the information around the periphery of the tumour. This might cause missed diagnosis of NVI due to the tumour edges associated with MVI and PNI.[16] As an example, Xu *et al.*[17] used radiomics features from multiscale volume of interest (VOI) of CECT to predict MVI in HCC. They showed that the peritumoural area contains information related to MVI. Unfortunately, there is limited radiomics research that investigates the relationship between the tumours with multiscale dilation and the prediction for MVI and PNI status in PDAC.

Positron-emission tomography/computed tomography (PET/CT) is a molecular imaging method that can non-invasively reflect tumour metabolism and molecular level changes in vivo. In recent years, many studies have demonstrated that 2-[^{18}F]-fluoro-2-deoxy-D-glucose (^{18}F-FDG) PET imaging has a unique value in staging, re-staging, therapeutic evaluation and prognosis prediction of multiple tumours such as breast cancer and lung adenocarcinoma.[18–20] These studies demonstrated that ^{18}F-FDG PET/CT-based radiomics was better at monitoring biological characteristics to reflect the status of tumour metabolism compared to other imaging methods such as CECT or MRI. In PDAC, >90% of tumours at PET/CT demonstrated foci of intense uptake.[21] Studies reported that the diagnostic sensitivity and accuracy of PET/CT for detecting PDAC are equivalent or superior to multidetector CT (MDCT) and MRI,[22–24] which could be attributed to the low-enhancing lesions of PDAC on contrast-enhanced CT and MRI; however, PET/CT takes advantage of increased glycolytic uptake for the segmentation of the tumours. According to a literature review, no study to date, has predicted the presence of MVI and PNI in PDAC using a ^{18}F-FDG PET/CT radiomics signature.

The present study investigated the use of ^{18}F-FDG PET/CT radiomics features extracted from the whole tumour and peritumoural region to detect the presence of MVI and PNI preoperatively in PDAC, which could help to provide more effective strategies for patients at high risk of NVI during the preoperative evaluation. The aim of the present study was to construct and validate a feasible prediction model from the multi-region VOIs together with other clinicopathological characteristics to predict preoperative MVI and PNI status in patients with PDAC.

Materials and methods

Patients

Preoperative ^{18}F-FDG PET/CT data was collected from 170 patients with PDAC between January 2013 and July 2018. The present study was approved by the Ethics Committee of Fudan University Shanghai Cancer Center (no. 1909207-14-1910) and all the data were analysed anonymously. The requirement for written informed consent was waived. The

inclusion criteria were as follows: (1) primary pancreatic lesions were surgically removed and histopathologically confirmed to be PDAC; (2) patients underwent ^{18}F-FDG PET/CT within 1 week before surgery; (3) patients did not receive any treatment related to tumours before ^{18}F-FDG PET/CT; (4) complete medical records and clinical characteristics were available. The exclusion criteria were as follows: (1) invalid ^{18}F-FDG PET/CT images; (2) lack of MVI and PNI results in the postoperative pathological reports; (3) presence of other malignant tumours; (4) incomplete clinical data. A total of 170 patients were included in the study.

Assessment of MVI and PNI status

The presence of MVI and PNI were determined by two pathologists, and the diagnoses were confirmed by another senior pathologist. MVI was defined by identifying a cluster of intravascular cancer cells away from the primary tumour that was visible only on microscopy.[6] The presence of PNI refers to the infiltration of tumour cells along the perineural space or into the perineural space from the weak part of the perineural space.[25]

Acquisition of ^{18}F-FDG PET/CT imaging

^{18}F-FDG PET/CT imaging was acquired on a whole-body PET/CT scanner (Biograph 16 HR, Siemens Medical Systems, Erlangen, Germany). Before ^{18}F-FDG administration (3.7 MBq/kg), the blood glucose levels of all the patients were $<$10 mmol/l. All patients fasted for at least 6 h prior to the injection and rested in a dimly lit room for 1 h after ^{18}F-FDG injection. Spiral CT was first performed with the range from the proximal thighs to calvarium. Parameters used in this study were as follows: 120 kV, 140 mA, pitch of 3.6, 0.5 seconds rotation time, and 5 mm section thickness). PET was then conducted immediately over the same extent. The acquisition time was 2$\sim$3 minutes per bed position. The acquired PET and CT images were reconstructed with a Gaussian-filter iterative method (iteration 4, subsets 8) and analysed on a workstation.

Acquisition of clinicopathological indicators

Ten clinicopathological indicators of significance were collected for pancreatic cancer to explore whether they have an auxiliary effect on the prediction of MVI and PNI status. The indicators include gender, age, tumour size (based on the longest diameter), location (Caput pancreatis, pancreatic body, pancreatic tail, multi-region (two or more sub-regions)), tumour differentiation (well-differentiated, moderately differentiated, poorly differentiated), mean standard uptake value (SUVmean), maximum standard uptake value (SUVmax), metabolic tumour volume (MTV), total lesion glycolysis (TLG) and preoperative CA19-9. MTV was measured using an absolute SUV threshold value of 2.5. TLG was calculated according to the formula: TLG $=$ MTV $\times$ SUVmean. Details of these parameters are listed in Table 1.

Radiomics analysis

The overview of the radiomics analysis is shown in Fig 1. Different sets of quantitative features that are related to MVI and PNI were extracted separately as biomarkers through radiomics analysis of PET/CT images and clinicopathological indicators, making it possible to predict invasion in a non-invasive manner.

VOI segmentation

Tumour volume was delineated manually and independently using the ITK-SNAP 3.8.0 (http://www.itksnap.org) by two nuclear medicine specialists, and the results were reviewed by another nuclear medicine specialist. Three experts were blinded to the clinical and pathological results. Disagreements were discussed until a consensus was reached. The original tumour volume ($VOI^{original}$) mainly reflects intra-tumoural heterogeneity. To extract information related to microvascular and nerve involvement in the periphery of the tumour appropriately, the delineated tumour was expanded by multiscale (3, 5, and 10 mm) through the dilation operation in binary mathematical morphology to obtain the dilated VOIs ($VOI^{dilated\_i}$, i $=$ 3, 5, 10). An example of the tumour segmentation and morphological dilation is shown in Fig 2. More information about data preprocessing is recorded in Electronic Supplementary Material Part I.

Feature extraction

Radiomics features were extracted from the $VOI^{original}$ and the $VOI^{dilated\_i}$ separately. The entire process was conducted using the PyRadiomics (https://github.com/AIM-Harvard/pyradiomics), which is an open-source Python package for the extraction of radiomics features from medical imaging.[26] This has been shown in the literature to extract various and complex radiomics features effectively.[18,27,28] Three types of features were extracted: shape, intensity, and texture. The shape features include elongation, flatness, etc. The extracted intensity features mainly include energy, entropy, etc. The second order and higher-order texture features were obtained from different grey-level matrices, including grey-level co-occurrence matrix (GLCM), grey-level run length matrix (GLRLM), grey-level size zone matrix (GLSZM), neighbouring grey-tone difference matrix (NGTDM) and grey-level dependence matrix (GLDM). Finally, 1,023 CT image features and 107 PET image features were extracted from each VOI. Reasons for the large difference in the number of PET and CT features and details of these characteristics (see Electronic Supplementary Material Table S1) are shown in Electronic Supplementary Material Part II.

Feature selection

Feature selection removes redundant and irrelevant information to obtain a smaller subset of features without significantly compromising the classification distribution and accuracy. For this work, a fast feature selection

Table 1
The clinicopathological characteristics of the patients.

Variables	MVI (−) (n=120)	MVI (+) (n=50)	p-Value (MVI)	PNI (−) (n=24)	PNI (+) (n=146)	p-Value (PNI)
Gender			0.952			0.941
Female	51 (30%)	21 (12.4%)		10 (5.9%)	62 (36.5%)	
Male	69 (40.6%)	29 (17%)		14 (8.2%)	84 (49.4%)	
Age (years)	62 (31–83)	60 (31–77)	<0.05*	62 (31–79)	61 (31–83)	0.506
Tumour size (cm)	3.2 (0.5–9)	3.5 (0.6–6.5)	0.655	3.5 (1.2–9)	3.2 (0.5–8.2)	0.741
Location			0.981			0.868
Caput pancreatis	65 (38.2%)	27 (15.9%)		12 (7.1%)	80 (47.1%)	
Pancreatic body	19 (11.2%)	7 (4.1%)		5 (2.9%)	21 (12.4%)	
Pancreatic tail	19 (11.2%)	9 (5.3%)		4 (2.4%)	24 (14.1%)	
Multi-region	17 (10.0%)	7 (4.1%)		3 (1.8%)	21 (12.4%)	
Tumour differentiation			1.000			0.176
Well-differentiated	18 (10.6%)	8 (4.7%)		6 (3.5%)	20 (11.8%)	
Moderately differentiated	93 (54.7%)	39 (22.9%)		18 (10.6%)	114 (67.1%)	
Poorly differentiated	9 (5.3%)	3 (1.8%)		0	12 (7.1%)	
SUVmean	3.415 (2.61–9.35)	3.43 (2.23–10.64)	0.897	3.465 (2.8–5.54)	3.42 (2.23–10.64)	0.360
SUVmax	5.68 (2.76–29.44)	5.63 (2.23–26.76)	0.874	5.93 (3.31–14.17)	5.605 (2.23–29.44)	0.347
MTV	14.15 (0.13–152.68)	7.9 (0.08–157.79)	0.065	12.13 (1.49–48.61)	12.725 (0.08–157.79)	0.971
TLG	48.195 (0.4–688.83)	28.835 (0.18–1561.77)	0.108	47.275 (4.17–215.6)	45.04 (0.18–1561.77)	0.858
Preoperative CA19-9	174.95 (<0.6～>1000)	292.35 (10.05～>1000)	0.159	206.55 (<0.6～>1000)	232.25 (<0.6～>1000)	0.746

For categorical variables, the number of samples and their percentages in all samples are provided; for continuous variables, the median and range are given. MVI, microvascular invasion; PNI, perineural invasion; SUV, standardised uptake value; MTV, metabolic tumour volume; TLG, total lesion glycolysis; CA19-9, carbohydrate antigen 19-9.

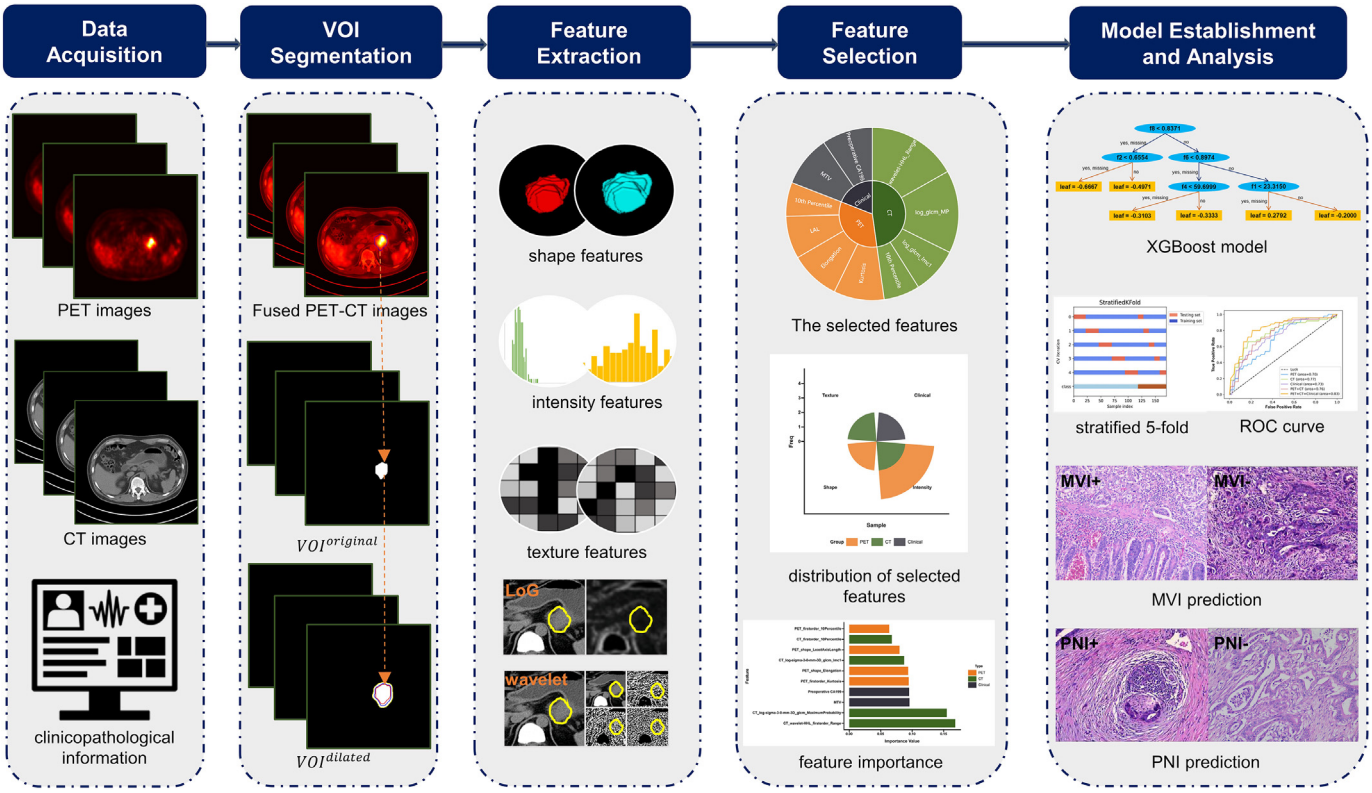

Figure 1 Overview of the radiomics analysis for MVI and PNI using PET/CT images of PDAC patients.

algorithm was employed named BoostARoota (https://github.com/chasedehan/BoostARoota) utilising eXtreme Gradient Boosting (XGBoost)[29] as the base model to select the features of PET, CT and clinicopathological parameters most relevant to MVI and PNI, respectively. BoostARoota has been adopted successfully as a feature-selection tool for the task of prediction of heart diseases[30] and sepsis.[31] The illustration and flowchart of BoostARoota are shown in Electronic Supplementary Material Part III and Fig. S1. Before performing feature selection, the problem of data imbalance was resolved through sampling, and the details were given in Electronic Supplementary Material Part IV.

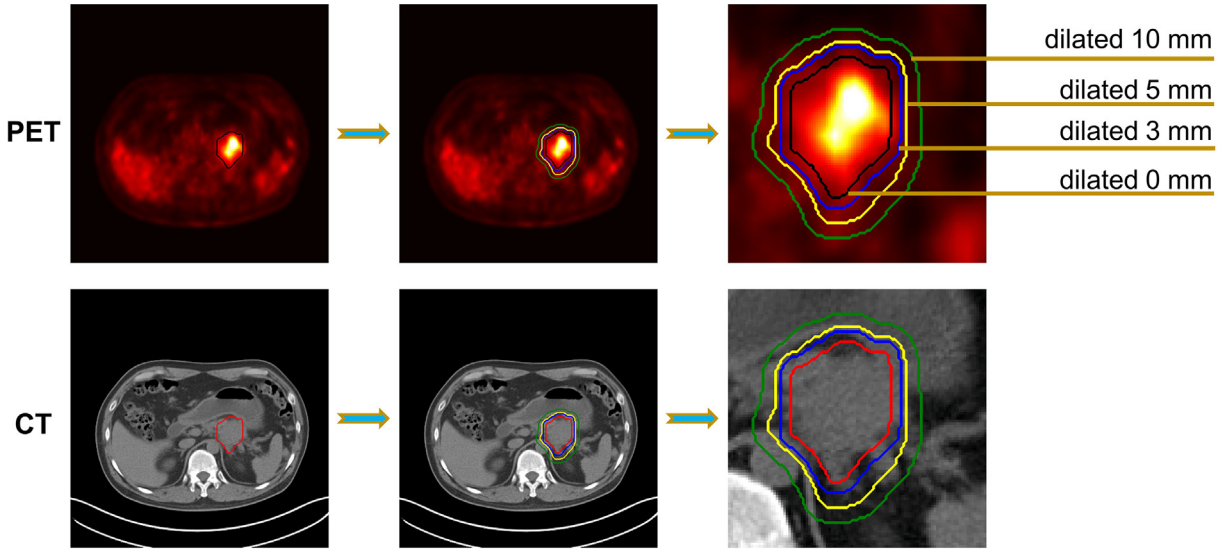

Figure 2 Schematic diagram of a tumour segmentation and morphological dilation. The black/red, blue, yellow, and green lines represent original mask delineation, 3 mm dilation, 5 mm dilation, and 10 mm dilation, respectively.

Development of the prediction model

Consistent with the work of Jiang *et al.*[32] and Chen *et al.*,[33] we also employed XGBoost as a classifier to explore the predictive power of the representative features of PET, CT, clinicopathological signatures, and their fusion for MVI and PNI. XGBoost is an implementation of gradient-boosted decision trees. In the experiment, a stratified fivefold cross-validation approach was adopted. In each cross-validation fold, the XGBoost was trained on 80% of samples and tested on an unseen subset of 20% of samples. The performance of the predictive models was evaluated by receiver operating characteristic (ROC) curves and area under the curve (AUC). Other evaluation indicators including accuracy, recall, precision, and F1 score were also calculated and presented in the results for a more comprehensive analysis. Details of the TRIPOD criteria are shown in Electronic Supplementary Material Table S4.

Statistical analysis

All statistical tests were performed using SPSS 25.0 (https://www.ibm.com/products/spss-statistics). The 10 clinicopathological characteristics were assessed to investigate their association with MVI and PNI separately. For categorical variables, Pearson's chi-square test or Fisher's exact test was performed where appropriate; for continuous variables, the Mann–Whitney *U*-test was performed as the data does not conform to normal distribution. All tests were two-sided, and *p*-values of <0.05 with a 95% confidence interval were considered statistically significant.

RESULTS

Patient characteristics

The clinicopathological characteristics of the patients are summarised in Table 1. MVI was present in 50 (29.41%) and PNI was present in 146 (85.88%) of 170 PDAC patients. The mean age of patients was 61.10 ± 8.77 years, ranging from 31 to 83 years. The age is significantly correlated to MVI status. In the following research, when the feature subset was filtered by the feature-selection algorithm, age was excluded. There were no significant differences correlated with MVI and PNI among all the other evaluated parameters.

Selected features

The radiomics characteristics from $VOI^{original}$ and $VOI^{dilated\_i}$ were analysed separately. The prediction results of AUC showed that features from $VOI^{dilated\_3}$ have stronger predictive ability (see Fig 3), so the radiomics features selected were all from $VOI^{dilated\_3}$.

For MVI prediction, four PET, four CT, and two clinicopathological features were selected. Among them, the features of PET images include two shape features (elongation and least axis length) and two intensity features (10th percentile and kurtosis). The features derived from CT images include two intensity features (10th percentile and Wavelet-HHL_firstorder_Range) and two texture features (Log-sigma-3-0-mm-3D_glcm_Imc1 and Log-sigma-3-0-mm-3D_glcm_MaximumProbability). Moreover, clinicopathological parameters including preoperative CA19-9 and MTV were selected. Detailed explanations and classification statistics of these features are shown in Electronic Supplementary Material Table S2 and Fig 4a, respectively. Feature importance analysis of selected features (see Fig 5a) showed that all PET/CT radiomics features and clinicopathological parameters were significant for MVI prediction. Wavelet_HHL_firstorder_Range was the most important feature with a value of 0.1684.

For PNI prediction, three PET and five CT features were selected and there was no contributing clinicopathological signatures. The PET image features included two shape

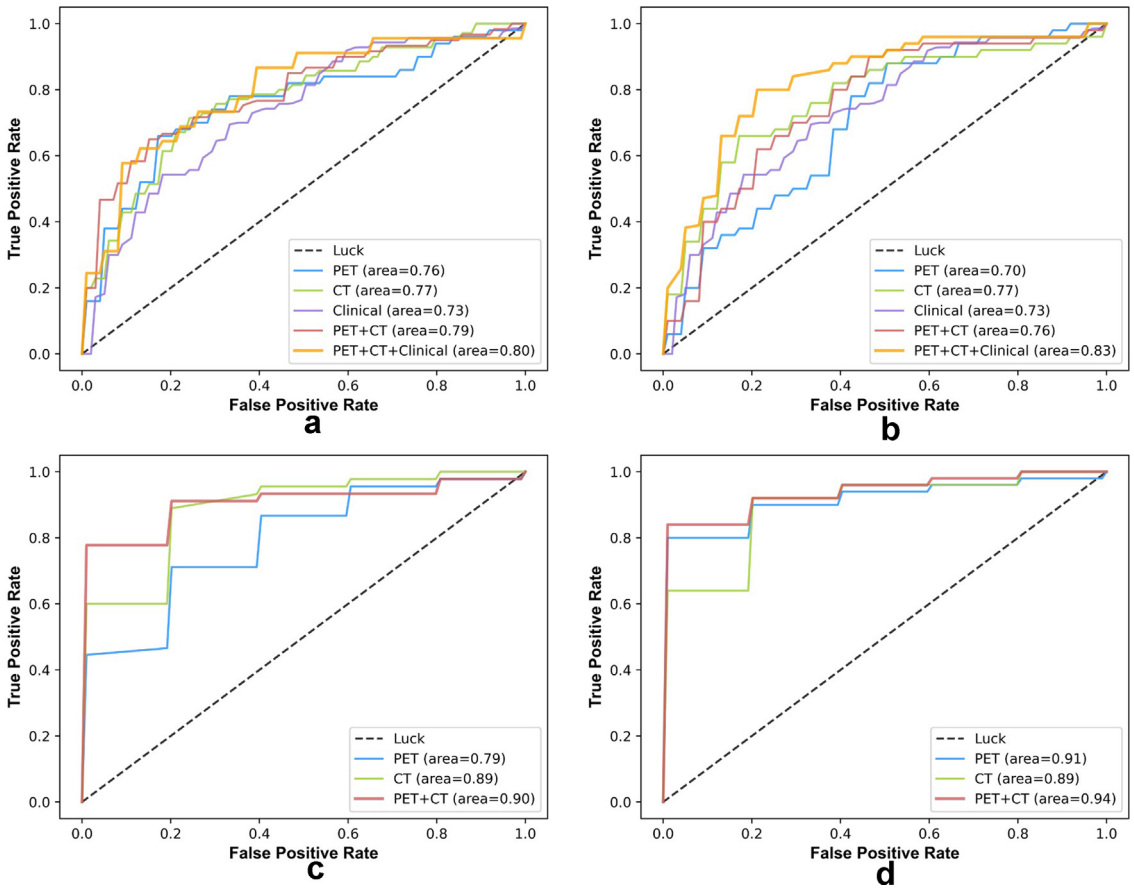

Figure 3 Comparison of ROC and AUC for MVI prediction and PNI prediction. (a) ROC curve of MVI prediction based on original VOI. (b) ROC curve of MVI prediction based on 3 mm-dilated VOI. (c) ROC curve of PNI prediction based on original VOI. (d) ROC curve of PNI prediction based on 3 mm-dilated VOI.

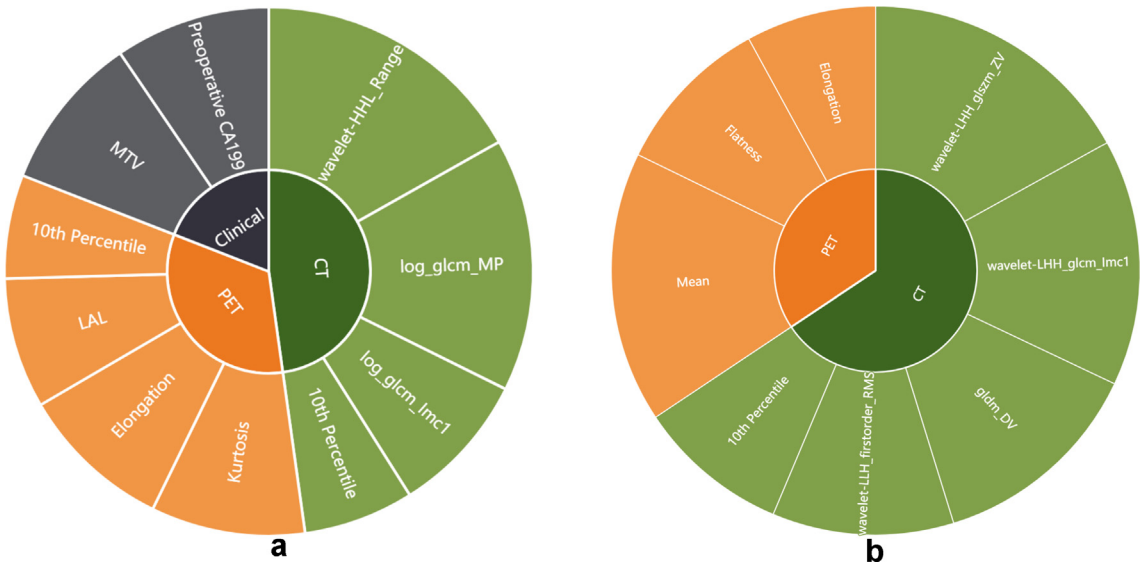

Figure 4 (a) Features of different modalities selected for MVI prediction. (b) Features of different modalities selected for PNI prediction.

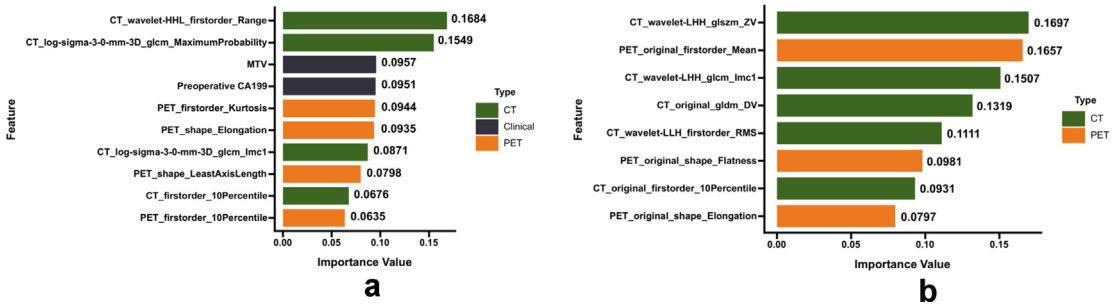

Figure 5 (a) Feature importance of MVI prediction based on 3 mm-dilated VOI. (b) Feature importance of PNI prediction based on 3 mm-dilated VOI.

features (elongation and flatness) and one intensity feature (mean). The valuable CT image features included two intensity features (10th percentile and Wavelet_LLH_firstorder_RootMeanSquared) and three texture features (gldm_DependenceVariance, wavelet_LHH_glcm_Imc1 and wavelet_LHH_glszm_ZoneVariance). Electronic Supplementary Material Table S3 and Fig 4b display the explanations and classification statistics of these features, respectively. Both the PET features and CT features are helpful for PNI prediction and wavelet_LHH_glszm_ZoneVariance is the most important feature with a value of 0.1697 (see Fig 5b).

Prediction results

The XGBoost model was trained on each monomodal feature subset and their fusion datasets. The complete numerical results were recorded in Tables 2 and 3. For MVI prediction, the maximum values of AUC derived from the model established on the dilated VOI of different scales were arranged in descending order: $VOI^{dilated\_3}$: 83.08% > $VOI^{dilated\_10}$: 81.5% > $VOI^{original}$: 79.81% > $VOI^{dilated\_5}$: 77.75%. For PNI prediction, the order is: $VOI^{dilated\_3}$: 94% > $VOI^{original}$: 90.67% > $VOI^{dilated\_5}$: 85.8% > $VOI^{dilated\_10}$: 85.2%. The model based on $VOI^{dilated\_3}$ showed better prediction performance than that based on $VOI^{original}$, and in most cases, the dilation of 5/10 mm made the prediction result worse (excessive volume may induce noise). Therefore, the ROC curve (see Fig 3) and the box plot of the comparison results of AUC were drawn based on the stratified fivefold cross-validation (see Electronic Supplementary Material Fig. S2) using on the $VOI^{original}$ and $VOI^{dilated\_3}$. Moreover, the ability to stratify MVI and PNI of the predictive models based on $VOI^{dilated\_3}$ were illustrated by representative cases (see Electronic Supplementary Material Fig. S3).

For MVI prediction, models based on the feature subset of only CT images performed better than those based on PET images or clinicopathological parameters for $VOI^{original}$ (the AUCs of CT, PET, clinicopathological were 77.1% versus 75.83% versus 73.3%) and $VOI^{dilated\_3}$ (the AUCs of CT, PET, clinicopathological were 77.42% versus 70.25% versus 73.3%). When combined the PET/CT radiomics features with clinicopathological parameters, the prediction result of AUC based on $VOI^{dilated\_3}$ was 3.27% higher than that based on

Table 2
The microvascular invasion (MVI) prediction performance of different feature subsets.

Modality	AUC	Accuracy	Recall	Precision	F1-score
MVI prediction based on **$VOI^{original}$**					
PET	75.83%	76.47%	75.17%	72.68%	73.41%
CT	77.10%	77.50%	70.67%	73.08%	71.39%
Clinical	73.30%	73.33%	66.05%	68.37%	66.62%
PET + CT	79.14%	80.50%	70.36%	80.84%	72.29%
PET + CT + clinical	79.81%	76.88%	72.42%	72.30%	72.08%
MVI prediction based on **$VOI^{dilated\_3}$**					
PET	70.25%	68.82%	59.25%	61.29%	59.04%
CT	77.42%	79.41%	74.33%	75.73%	74.24%
PET + CT	75.75%	72.35%	68.17%	68.82%	67.50%
PET + CT + clinical	83.08%	78.82%	75.08%	75.50%	74.59%
MVI prediction based on **$VOI^{dilated\_5}$**					
PET	68.25%	67.06%	63.25%	62.15%	61.95%
CT	73.08%	71.18%	63.83%	65.97%	64.29%
PET + CT	77.75%	78.24%	72.33%	74.28%	72.81%
PET + CT + clinical	76.25%	75.29%	71.42%	71.25%	70.88%
MVI prediction based on **$VOI^{dilated\_10}$**					
PET	81.50%	77.65%	72.50%	76.03%	72.69%
CT	73.92%	75.29%	70.25%	69.65%	69.55%
PET + CT	77.67%	78.24%	75.83%	74.84%	74.76%
PET + CT + clinical	78.08%	77.65%	73.67%	74.24%	73.02%

AUC, area under the curve; VOI, volume of interest; PET, positron-emission tomography; CT, computed tomography.

Table 3
The perineural invasion (PNI) prediction performance of different feature subsets.

Modality	AUC	Accuracy	Recall	Precision	F1-score
PNI prediction based on **$VOI^{original}$**					
PET	79.33%	74.29%	70.22%	73.32%	70.60%
CT	88.89%	87.14%	85.56%	86.49%	85.26%
PET + CT	90.67%	88.57%	88.44%	87.97%	87.76%
PNI prediction based on **$VOI^{dilated\_3}$**					
PET	91.60%	88%	89%	86.62%	87.01%
CT	89.60%	88%	88%	87.12%	86.89%
PET + CT	94%	89.33%	90%	87.81%	88.35%
PNI prediction based on **$VOI^{dilated\_5}$**					
PET	85.80%	78.67%	79%	76.68%	76.74%
CT	82.20%	73.33%	71%	72.64%	70.31%
PET + CT	84.80%	77.33%	73%	74.85%	73.42%
PNI prediction based on **$VOI^{dilated\_10}$**					
PET	75.20%	76%	72%	72.15%	71.76%
CT	85.20%	78.67%	78%	78.19%	76.62%
PET + CT	78%	76%	75%	74.76%	73.47%

AUC, area under the curve; VOI, volume of interest; PET, positron-emission tomography; CT, computed tomography.

$VOI^{original}$ and reached the optimal performance (see Fig 3a and b, Electronic Supplementary Material Fig. S2a and Table 2).

For PNI prediction, the feature subset extracted from the $VOI^{dilated\_3}$ has stronger predictive ability than the feature subset extracted from the $VOI^{original}$ whether it is from PET (AUCs were 91.6% versus 79.33%), CT (AUCs were 89.6% versus 88.89%) or multimodal PET/CT (AUCs were 94% versus 90.67%). Moreover, the model based on the feature subset of multimodal PET/CT outperformed the others (see Fig 3c and d, Electronic Supplementary Material Fig. S2b and Table 3).

Discussion

The present study developed a radiomics predictive model using PET/CT images and clinicopathological parameters for preoperative prediction of MVI and PNI status in PDAC. The present results demonstrated that the radiomics predictive model using preoperative ^{18}F-FDG PET and CT features coupled with clinical factors to identify MVI status achieved an AUC of 79.81% and 83.08% from the $VOI^{original}$ and $VOI^{dilated\_3}$ respectively. Additionally, PET and CT radiomics features from $VOI^{dilated\_3}$ also provided the best prediction results than the other three strategies for PNI prediction. The present findings indicate that the capability of the ^{18}F-FDG PET/CT radiomics model can be used as a dependable marker to predict the status of MVI and PNI in patients with PDAC before surgery.

MVI is not uncommon in PDAC as it was identified in 29% of patients in the present study with higher rates in the retrospective analysis reported by Yamada *et al.*,[6] reflecting the rapid progress and poorer prognosis of the disease. Accurate preoperative estimation of MVI status plays a vital role in guiding perioperative therapeutic decisions for patients with PDAC.[34] Increasingly, studies have focused on the relationships between radiomics features and MVI status,[33,35] but the prediction model for MVI in PDAC based on PET/CT radiomics features had not been well established. In the present study, one texture feature, one intensity feature, and MTV were the most important components for predicting MVI. This finding was partially coincident with the result of Yang *et al.*,[36] suggesting that the texture features and the discrete degree of grey level in tumours were important for MVI prediction. Previous studies[17,37] have shown that shape features, such as tumour capsule or margin, were significantly related to the diagnosis of MVI status based on CECT or CEMRI images; however, in the present study, shape features only accounts for 17.33% amongst the feature contributions. The reason for this difference may be that the CT images are unenhanced and the resolution of PET images is relatively low in PET/CT, which can only depict limited shape information.

The incidence of PNI has been reported to be extremely high, with up to 80%–100%.[38] Patients with PNI have a higher recurrence rate and mortality of PDAC after surgery than that of patients without PNI.[39,40] Therefore, evaluating the PNI status of PDAC and intervening as early as possible to reduce the risk of recurrence and metastasis is necessary. The present risk model, comprising of three PET features and five CT features to predict PNI of PDAC, resulted in an AUC of 90.67% and 94% in the $VOI^{original}$ and $VOI^{dilated\_3}$ group, respectively. Both PET and CT radiomics predictors have positive importance to increase the model accuracy. Thus, the combination of CT and PET of ^{18}F-FDG metabolism can improve the prediction efficiency more than any single modality model; however, clinicopathological characteristics in the present study had no contribution to the model. Texture features of CT and intensity features of PET were the most valuable indicators in the model predictions, indicating that the average grey-level intensity and the distribution, as well as local tumour heterogeneity in the image are closely related with PNI. Wavelet_LHH_glszm_ZoneVariance and wavelet_LHH_glcm_Imc1 were the features selected from the CT images. These are consistent with the selected features of SZM GL non-uniformity and CM dissimilarity in the work of Li *et al.*,[41] all of which express the non-uniformity of the image grey area.

The aggressive behaviours of the target tumour cannot be observed directly from both intra-tumoural and peritumoural regions. In addition, the main challenge of the current imaging methods or radiomics analysis to predict NVI is the precise determination of the tumour boundary. The $VOI^{dilated\_3}$ radiomics predictors achieved the highest value of the AUC both for MVI and PNI prediction and was superior to features derived from $VOI^{original}$, $VOI^{dilated\_5}$, $VOI^{dilated\_10}$. Similarly, Xu *et al.*[17] reported that MVI-related radiomics scores at the $VOI^{penumbra}$ (VOI at 5 mm distance from the tumour surface) were different from scores at the VOI^{entire} (same as our $VOI^{original}$), but were not superior. This is not consistent with the present research, finding that 3 mm dilation was the most appropriate boundary potentially associated to tumour MVI and PNI information in PDAC. The reason may be that the research of Xu *et al.* focused on predicting the MVI status of HCC based on CECT and there are differences between the tumour-related feature information extracted from the CECT images and the PET/CT images. The present approach provides new insights into the contribution of ^{18}F-FDG PET/CT radiomics to overcome the negative affect on the prediction caused by single VOI features and subjective visual assessment.

The present study has some limitations. First, the study was a single-centred, retrospective study with limited samples. Second, only patients who underwent surgery and had histopathologically confirmed PDAC were included. There is a selection bias against those patients with high-risk features that would not undergo surgery, such as the patients who underwent neoadjuvant treatment. There is certainly room to improve the study of preoperative invasion prediction based on multiscale dilation tumours derived from PET/CT imaging. In future studies, multicentre data will be obtained, and radiomics will be combined with deep learning to realise fully automated analysis of the entire process from tumour segmentation to invasion prediction and obtain stronger evidence of the significance of ^{18}F-FDG PET/CT radiomics in patients with PDAC.

In conclusion, the ^{18}F-FDG PET/CT-derived radiomics features combined with clinicopathological indicators could be used as a non-invasive biomarker and exhibited instructive value for preoperative prediction of MVI and PNI status in patients with PDAC. The present approach using peritumoural radiomics features from the 3 mm dilation of VOI in the ^{18}F-FDG PET/CT images achieved the highest performance in the prediction of MVI and PNI preoperatively. This prediction model can inspire more research related to NVI prediction for the treatment of PDAC patients.

Declaration of competing interest

The authors declare that they have no known competing financial interests or personal relationships that could have appeared to influence the work reported in this paper.

Acknowledgements

This study was supported by National Natural Science Foundation of China (no. 81771861), Science and Technology Commission of Shanghai Municipality (no. 19142202100), SJTU Global Strategic Partnership Fund (no. 2021 SJTU-USyd).

Appendix A. Supplementary data

Supplementary data to this article can be found online at https://doi.org/10.1016/j.crad.2023.05.007.

References

1. Ilic M, Ilic I. Epidemiology of pancreatic cancer. *World J Gastroenterol* 2016;**22**(44):9694–705.
2. Allemani C, Matsuda T, Di Carlo V, *et al*. Global surveillance of trends in cancer survival 2000-14 (CONCORD-3): analysis of individual records for 37 513 025 patients diagnosed with one of 18 cancers from 322 population-based registries in 71 countries. *Lancet* 2018;**391**(10125):1023–75.
3. Matsumoto I, Murakami Y, Shinzeki M, *et al*. Proposed preoperative risk factors for early recurrence in patients with resectable pancreatic ductal adenocarcinoma after surgical resection: a multi-center retrospective study. *Pancreatology* 2015;**15**(6):674–80.
4. Hirono S, Kawai M, Okada KI, *et al*. Pancreatic neck cancer has specific and oncologic characteristics regarding portal vein invasion and lymph node metastasis. *Surgery* 2016;**159**(2):426–40.
5. Takahashi H, Ohigashi H, Ishikawa O, *et al*. Perineural invasion and lymph node involvement as indicators of surgical outcome and pattern of recurrence in the setting of preoperative gemcitabine-based chemoradiation therapy for resectable pancreatic cancer. *Ann Surg* 2012;**255**(1):95–102.
6. Yamada M, Sugiura T, Okamura Y, *et al*. Microscopic venous invasion in pancreatic cancer. *Ann Surg Oncol* 2018;**25**(4):1043–51.
7. Kimbrough CW, St Hill CR, Martin RCG, *et al*. Tumour-positive resection margins reflect an aggressive tumour biology in pancreatic cancer. *J Surg Oncol* 2013;**107**(6):602–7.
8. Tsuchiya N, Matsuyama R, Murakami T, *et al*. Risk factors associated with early recurrence of borderline resectable pancreatic ductal adenocarcinoma after neoadjuvant chemoradiation therapy and curative resection. *Anticancer Res* 2019;**39**(8):4431–40.
9. Groot VP, Gemenetzis G, Blair AB, *et al*. Defining and predicting early recurrence in 957 patients with resected pancreatic ductal adenocarcinoma. *Ann Surg* 2019;**269**(6):1154–62.
10. Yeh R, Steinman J, Luk L, *et al*. Imaging of pancreatic cancer: what the surgeon wants to know. *Clin Imag* 2017;**42**:203–17.
11. Lambin P, Leijenaar RTH, Deist TM, *et al*. Radiomics: the bridge between medical imaging and personalized medicine. *Nat Rev Clin Oncol* 2017;**14**(12):749–62.
12. Blanc-Durand P, Van Der Gucht A, Jreige M, *et al*. Signature of survival: a (18)F-FDG PET based whole-liver radiomic analysis predicts survival after (90)Y-TARE for hepatocellular carcinoma. *Oncotarget* 2018;**9**(4):4549–58.
13. Peng J, Zhang J, Zhang QF, *et al*. A radiomics nomogram for preoperative prediction of microvascular invasion risk in hepatitis B virus-related hepatocellular carcinoma. *Diagn Interv Radiol* 2018;**24**(3):121–7.
14. Chen H, Zhao L, Fu K, *et al*. Integrin alphavbeta3-targeted radionuclide therapy combined with immune checkpoint blockade immunotherapy synergistically enhances anti-tumour efficacy. *Theranostics* 2019;**9**(25):7948–60.
15. Chen JY, Chen Y, Zheng DC, *et al*. Pretreatment MR-based radiomics nomogram as potential imaging biomarker for individualized assessment of perineural invasion status in rectal cancer. *Abdom Radiol* 2021;**46**(3):847–57.
16. Kusano Hironori, Han Jing, Bulthuis Marian, *et al*. Liver cancer. *Hepatology* 2013;**58**(Suppl. 1):1213A–76A.
17. Xu X, Zhang HL, Liu QP, *et al*. Radiomic analysis of contrast-enhanced CT predicts microvascular invasion and outcome in hepatocellular carcinoma. *J Hepatol* 2019;**70**(6):1133–44.
18. Li P, Wang X, Xu C, *et al*. 18)F-FDG PET/CT radiomic predictors of pathologic complete response (pCR) to neoadjuvant chemotherapy in breast cancer patients. *Eur J Nucl Med Mol Imaging* 2020;**47**(5):1116–26.
19. Liu Q, Sun D, Li N, *et al*. Predicting EGFR mutation subtypes in lung adenocarcinoma using ^{18}F-FDG PET/CT radiomic features. *Translat Lung Cancer Res* 2020;**9**(3):549.
20. Ren C, Zhang J, Qi M, *et al*. Machine learning based on clinico-biological features integrated (18)F-FDG PET/CT radiomics for distinguishing squamous cell carcinoma from adenocarcinoma of lung. *Eur J Nucl Med Mol Imaging* 2021;**48**(5):1538–49.
21. Halbrook CJ, Lyssiotis CA. Employing metabolism to improve the diagnosis and treatment of pancreatic cancer. *Cancer Cell* 2017;**31**(1):5–19.
22. Best LM, Rawji V, Pereira SP, *et al*. Imaging modalities for characterising focal pancreatic lesions. *Cochrane Database Syst Rev* 2017;**4**:CD010213.
23. Kauhanen SP, Komar G, Seppanen MP, *et al*. A prospective diagnostic accuracy study of ^{18}F-fluorodeoxyglucose positron emission tomography/computed tomography, multidetector row computed tomography, and magnetic resonance imaging in primary diagnosis and staging of pancreatic cancer. *Ann Surg* 2009;**250**(6):957–63.
24. Ghaneh P, Hanson R, Titman A, *et al*. PET-PANC: multicentre prospective diagnostic accuracy and health economic analysis study of the impact of combined modality ^{18}fluorine-2-fluoro-2-deoxy-d-glucose positron emission tomography with computed tomography scanning in the diagnosis and management of pancreatic cancer. *Health Technol Assess* 2018;**22**(7):1–114.
25. Liebig C, Ayala G, Wilks JA, *et al*. Perineural invasion in cancer: a review of the literature. *Cancer* 2009;**115**(15):3379–91.
26. van Griethuysen Jjm, Fedorov A, Parmar C, *et al*. Computational radiomics system to decode the radiographic phenotype. *Cancer Res* 2017;**77**(21):e104–7.
27. Xing H, Hao Z, Zhu W, *et al*. Preoperative prediction of pathological grade in pancreatic ductal adenocarcinoma based on (18)F-FDG PET/CT radiomics. *EJNMMI Res* 2021;**11**(1):19.
28. Zhang YC, Lobo-Mueller EM, Karanicolas P, *et al*. Improving prognostic performance in resectable pancreatic ductal adenocarcinoma using radiomics and deep learning features fusion in CT images. *Sci Rep-Uk* 2021;**11**(1).
29. Chen TQ, Guestrin C. XGBoost: a scalable tree boosting system. In: *Kdd'16: Proceedings of the 22nd ACM SIGKDD International Conference on Knowledge Discovery and Data Mining*; 2016. p. 785–94.
30. Anuradha P, David VK. Feature selection using ModifiedBoostARoota and prediction of heart diseases using Gradient Boosting algorithms. In: *2021 IEEE Int Conf Comput Commun Intell Syst (ICCCIS)*; 2021. p. 19–23.

31. Zabihi M, Kiranyaz S, Gabbouj M. Sepsis prediction in intensive care unit using ensemble of XGboost models. In: *2019 Computing in cardiology (CinC). IEEE***1–4**; 2019.
32. Jiang YQ, Cao SE, Cao S, *et al*. Preoperative identification of microvascular invasion in hepatocellular carcinoma by XGBoost and deep learning. *J Cancer Res Clin Oncol* 2021;**147**(3):821–33.
33. Chen Y, Xia Y, Tolat PP, *et al*. Comparison of conventional gadoxetate disodium-enhanced MRI features and radiomics signatures with machine learning for diagnosing microvascular invasion. *AJR Am J Roentgenol* 2021;**216**(6):1510–20.
34. Delpero JR, Jeune F, Bachellier P, *et al*. Prognostic value of resection margin involvement after pancreaticoduodenectomy for ductal adenocarcinoma: updates from a French prospective multicenter study. *Ann Surg* 2017;**266**(5):787–96.
35. Chong HH, Yang L, Sheng RF, *et al*. Multi-scale and multi-parametric radiomics of gadoxetate disodium-enhanced MRI predicts microvascular invasion and outcome in patients with solitary hepatocellular carcinoma </= 5 cm. *Eur Radiol* 2021;**31**(7):4824–38.
36. Yang L, Gu D, Wei J, *et al*. A radiomics nomogram for preoperative prediction of microvascular invasion in hepatocellular carcinoma. *Liver Cancer* 2019;**8**(5):373–86.
37. Ma X, Liu L, Fang J, *et al*. MRI features predict microvascular invasion in intrahepatic cholangiocarcinoma. *Cancer Imaging* 2020;**20**(1):40.
38. Keleg S, Buchler P, Ludwig R, *et al*. Invasion and metastasis in pancreatic cancer. *Mol Cancer* 2003;**2**:14.
39. Bapat AA, Hostetter G, Von Hoff DD, *et al*. Perineural invasion and associated pain in pancreatic cancer. *Nat Rev Cancer* 2011;**11**(10):695–707.
40. Wang J, Chen Y, Li X, *et al*. Perineural invasion and associated pain transmission in pancreatic cancer. *Cancers (Basel)* 2021;**13**(18).
41. Li Y, Eresen A, Shangguan JJ, *et al*. Preoperative prediction of perineural invasion and KRAS mutation in colon cancer using machine learning. *J Cancer Res Clin* 2020;**146**(12):3165–74.